JTTEE5 17:692–699
DOI: 10.1007/s11666-008-9227-8
1059-9630/$19.00 © ASM International

Peer Reviewed

Optimization of Solution Precursor Plasma Spray Process by Statistical Design of Experiment

Y. Wang and T.W. Coyle

(Submitted May 14, 2008; in revised form September 15, 2008)

The solution precursor plasma spray (SPPS) process, in which a solution precursor of the desired resultant material is fed into a plasma jet by atomizing gas or high pressure, was developed in the 1990s and has been studied extensively since then. Recently, it has been shown that the SPPS process is suitable for deposition of porous electrodes for solid oxide fuel cells (SOFC). High efficiency SOFC requires electrodes with 30-40% porosity. Due to the complexity of the SPPS process and the large number of processing parameters, it is difficult to investigate the effect of each parameter on the two important properties, i.e., coating porosity and deposition efficiency, separately. Design of experiments can use a small number of experimental runs to analyze the effect of each processing parameter on the properties of the fabricated product, after which the processing parameter combinations for fabricating a target product can be found. In this project, a small central composite design (CCD), a second-order statistical model, was used to analyze and optimize the SPPS process for Ni-YSZ anode deposition. The processing parameters investigated include: (1) Hydrogen flow rate, which determines arc voltage, (2) Current, (3) Solute flow rate, (4) Solution concentration, (5) Distance between nozzle and gun, and (6) Stand off distance. The effects of the selected processing parameters were analyzed, and the resultant model was used to select a combination of processing parameters, which produced a coating with the desired characteristics.

Keywords Electrode, Ni-YSZ anode, Solid oxide fuel cell (SOFC), Solution precursor plasma spray (SPPS)

1. Introduction

The solution precursor plasma spray (SPPS) process, in which a solution precursor was injected into a plasma jet to synthesize product materials and deposit coatings simultaneously, was developed in the 1990s and has been investigated extensively since then (Ref 1-5). Recently SPPS by direct current arc plasma spraying (DC-SPPS) has been used to produce coatings with high porosity (Ref 6, 7), suitable for use as solid oxide fuel cell (SOFC) electrode and sensor applications. Since a large number of processing parameters are involved in the SPPS process, it is difficult to establish relationships between the processing parameters and the properties of the deposited coatings. However, many applications require a particular property or combination of properties to be within a specific range, for example, high-quality electrodes for SOFC application require the porosity in the deposited coating to be in the range of 30-40%. In addition, to reduce cost and production time, the deposition efficiency of the SPPS process should be as high as possible. Therefore, deposition of coatings with one or several target properties and high-deposition efficiency is required from a practical SPPS process.

Statistical design of experiments is a mathematical method to establish the relations between the properties (responses) of a product and the processing parameters (factors) used in fabricating it, after which the processing parameter combination for making a target product could be found (optimization) (Ref 8, 9). The relations are obtained by measuring the properties of the product fabricated with different combinations of the processing parameters (the experimental design matrix) and employing statistical techniques to analyze the measured properties.

The classical approach of investigating the effect of each parameter on the final coatings one by one requires a large number of experimental runs because of the large number of processing parameters involved in the SPPS process. Design of experiments can use a small number of experimental runs to obtain a large amount of information about the effects of the processing parameters on the

This article is an invited paper selected from presentations at the 2008 International Thermal Spray Conference and has been expanded from the original presentation. It is simultaneously published in *Thermal Spray Crossing Borders, Proceedings of the 2008 International Thermal Spray Conference*, Maastricht, The Netherlands, June 2-4, 2008, Basil R. Marple, Margaret M. Hyland, Yuk-Chiu Lau, Chang-Jiu Li, Rogerio S. Lima, and Ghislain Montavon, Ed., ASM International, Materials Park, OH, 2008.

Y. Wang and **T.W. Coyle**, Centre for Advanced Coating Technologies, Department of Materials Science and Engineering, University of Toronto, Toronto, ON, Canada. Contact e-mail: youliang.wang@cnrc-nrc.gc.ca.

coating's properties. This approach has been widely employed to identify desirable process conditions for the deposition of thermal spray coatings, for example the vacuum plasma spray deposition of alumina, nickel-base alloys and tungsten carbide/cobalt cermet coatings (Ref 10), the high-velocity oxy fuel (HVOF) spraying of chromium carbide/nickel chromium coatings (Ref 11) and air plasma spray deposition of Ni-based superalloy (Ref 12). The application of statistical design of experiments to the development of thermal spray coatings has been reviewed recently (Ref 13).

In this article a small central composite design (CCD) (Ref 14), a second-order model, was used to investigate the effects of six processing parameters on coating porosity and deposition efficiency in the DC-SPPS process. The parameters investigated were: (1) Hydrogen flow rate, which determines arc voltage, (2) Current, (3) Solute flow rate, (4) Solution concentration, (5) Distance between nozzle and gun, (6) Stand off distance. The effects of the selected parameters were analyzed, and the SPPS process was successfully optimized.

2. DC-SPPS Setup, Solution Precursor, and Substrates

The DC-SPPS setup consists of a solution precursor feeder system, a solution atomizer-injector (nozzle), an atmospheric plasma spray system, and a sample holder (Ref 15). The solution precursor feeder system delivers measured quantities of the solution precursor to the nozzle fixed in front of the plasma torch, which produces atomized droplets of the precursor and injects them into the high-temperature plasma jet. A SG-100 torch (Miller Thermal) mounted on a robot was used. The solution precursor was made by adding distilled water to the mixture of $ZrOCl_2 \cdot 8H_2O$, $Y(NO_3)_3 \cdot 6H_2O$, and $Ni(NO_3)_3 \cdot 6H_2O$. The planned resultant material is 8YSZ-40 vol.%Ni (Ref 6, 15). Sintered partially stabilized zirconia discs with a diameter of 2 cm were used as substrates.

3. Optimization of SPPS Process for SOFC Anode Deposition

3.1 Small Central Composite Design

Central composite design (CCD) is the most popular response surface method (RSM) design (Ref 8, 9). A CCD has three groups of design points (1) two-level factorial or fractional factorial design points; (2) axial or star points; and (3) center points as shown in Fig. 1 Generally, the two level factorial points of the CCD are used to select critical factors first while the star points and center points are added to evaluate the curvature of the response surface and experimental error. Each factor in a CCD can have five levels. However, if the λ in Fig. 1 is set to 1, three levels for each factor can be used to get the well-known face-centered cubic array (FCC). When the number of

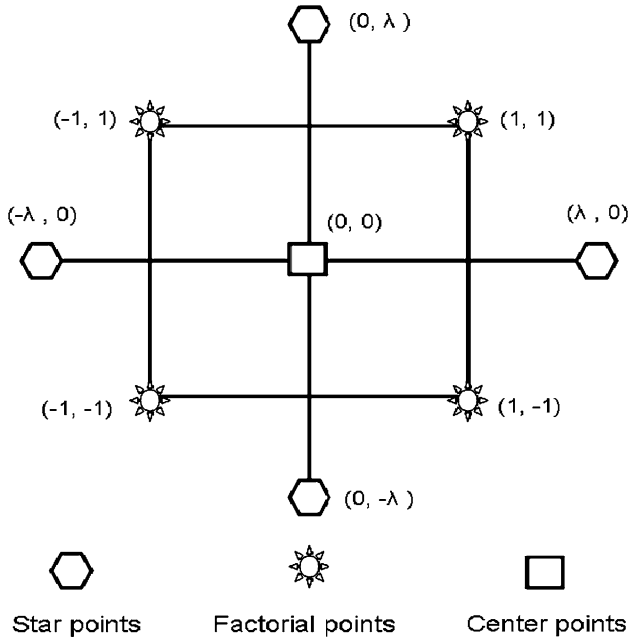

Fig. 1 Generation of a central composite design for two factors

factors is large, it is not necessary to run all combinations of factors. The factorial part of the design can be run in a fraction of the total number of available points. Standard CCDs may include any regular fractional factorial with a resolution of at least V, by which all the main effects and two factor interactions can be estimated.

If the experiment is expensive, small composite designs (SCDs), created by Hartley in 1959 (Ref 14), are alternatives to the standard CCDs. For the SCDs, the factorial part is not a regular fractional factorial of at least resolution V (Ref 14), but a special resolution III fractional factorial. Although by the resolution III factorial itself the main effects may be aliased with two factor interactions, the SCDs can give second-order models of the response. For *cubic* designs, all factors have three levels and the axial parts of the SCD have $\lambda = 1$.

3.2 Small Composite Design for Deposition of Ni-YSZ Anodes

All six processing parameters, including secondary plasma gas flow rate (HydrogenFR), which determines the gun arc voltage, gun current (I), solution precursor solute flow rate (SoluteFR), solution precursor concentration (SolutionC), distance between nozzle and gun (Distance-NG), and standoff distance (StandOD) were included in the small CCD. The design consisted of 34 experiments with 6 repeated center points as shown in Table 1. Each factor has three levels; therefore, the small central composite matrix is a face-centered (six dimensional) *cube*. The 34 deposition experiments are randomly distributed in the matrix to reduce the effect of systematic errors. In addition to the processing parameter values displayed in the matrix, the primary plasma gas (argon) flow rate was 62 l/min for all the runs; the atomizing gas pressure for different nozzle

Table 1 Small central composite design matrix for Ni-YSZ anode deposition

Std	Run	HydrogenFR	I	SoluteFR	SolutionC	DistanceNG	StandOD	EfficiencyR	Porosity
Unit		L/min	A	g/min	M	cm	cm	g	Area % ± std dev
6	1	3	570	7	0.5	0.3	8	0.134	47 ± 1.2
12	2	3	570	4	0.25	1.3	6	0.193	37 ± 2.1
19	3	2	600	5.5	0.375	0.8	7	0.071	35 ± 2.8
18	4	2	600	5.5	0.375	0.8	7	0.048	34 ± 0.3
2	5	3	630	7	0.25	1.3	6	0.149	33 ± 2.0
16	6	1	570	4	0.25	0.3	6	0.109	32 ± 1.6
7	7	1	630	7	0.25	0.3	6	0.071	30 ± 3.3
1	8	3	630	7	0.5	0.3	6	0.140	40 ± 2.4
8	9	3	630	4	0.25	1.3	8	0.057	29 ± 0.9
11	10	1	630	4	0.25	0.3	8	0.055	44 ± 2.5
20	11	2	600	5.5	0.375	0.8	7	0.064	34 ± 4.0
10	12	1	570	7	0.25	0.3	8	0.099	51 ± 1.5
13	13	1	570	4	0.5	1.3	6	0.152	35 ± 1.1
4	14	3	570	7	0.25	1.3	8	0.074	41 ± 1.8
14	15	1	570	7	0.5	1.3	8	0.252	47 ± 0.8
5	16	1	630	4	0.5	1.3	8	0.159	29 ± 0.7
9	17	3	570	4	0.5	0.3	6	0.137	42 ± 2.2
3	18	3	630	4	0.5	0.3	8	0.075	35 ± 2.1
15	19	1	630	7	0.5	1.3	6	0.180	43 ± 1.1
17	20	2	600	5.5	0.375	0.8	7	0.069	37 ± 1.6
34	21	2	600	5.5	0.375	0.8	7	0.072	36 ± 2.3
25	22	2	600	4	0.375	0.8	7	0.072	36 ± 0.4
23	23	2	570	5.5	0.375	0.8	7	0.079	38 ± 0.7
33	24	2	600	5.5	0.375	0.8	7	0.064	34 ± 2.8
22	25	3	600	5.5	0.375	0.8	7	0.076	29 ± 0.8
32	26	2	600	5.5	0.375	0.8	8	0.093	41 ± 0.4
26	27	2	600	7	0.375	0.8	7	0.117	33 ± 2.0
29	28	2	600	5.5	0.375	0.3	7	0.073	32 ± 2.1
30	29	2	600	5.5	0.375	1.3	7	0.099	33 ± 0.8
27	30	2	600	5.5	0.25	0.8	7	0.079	37 ± 1.8
24	31	2	630	5.5	0.375	0.8	7	0.093	34 ± 1.0
31	32	2	600	5.5	0.375	0.8	6	0.144	39 ± 1.6
28	33	2	600	5.5	0.5	0.8	7	0.106	40 ± 0.3
21	34	1	600	5.5	0.375	0.8	7	0.108	42 ± 2.5

positions was adjusted so that circular deposit footprints were generated on the substrates when the gun was held stationary. The duration of each deposition run was selected to compensate for the different amounts of solute consumed per minute due to the variations in solute flow rate levels, ensuring that the same total amount of solute was injected into the plasma jet over the course of each run.

Two responses were selected as the basis for the optimization. The porosity of the fabricated coating (Porosity) is one of the most important characteristics of the microstructure for SOFC performance and was found in the preliminary experiments to be the microstructural feature most sensitive to variations in deposition parameters. Deposition efficiency (EfficiencyR) was chosen because of its practical importance in production efficiency.

3.3 Experimental Data and Statistical Analysis

The 34 samples were deposited with a plasma gun scan speed 9.3 cm/s, scan length of 10 cm, and spray duration of 4 min, 5 min and 6 sec, and 7 min for the high, middle, and low solute flow rate levels, respectively. The deposition efficiency (EfficiencyR) in Table 1 is the weight gain (g) of the zirconia substrate discs. This is a relative measure valid only within this study since it depends on the substrate size, the amount of solute consumed, and other experimental conditions. The porosities (Porosity) in Table 1 were estimated by image analysis of SEM images of the polished cross sections of sintered and reduced coatings with the commercial software Clemex Vision PE 3.5. The polished cross sections for SEM observation were made by cutting the samples with a high-speed diamond saw (Clemex, Brillant 221), and then mounting the cut samples in a low-viscosity castable mounting resin using a vacuum impregnation setup. The analysis of the experimental data was done using Design Expert 7.0.2 (Ref 16). A detailed background of the data analysis procedures is described in Ref 8, 9.

3.4 Analysis Results

3.4.1 Quadratic Model for Deposition Efficiency. A six variable quadratic model including all 28 terms was fit to the 34 values of deposition efficiency (EfficiencyR) in Table 1. Tests on individual regression coefficients were done with $\alpha = 0.1$ in the t test statistic described in Ref 9. The terms found not to be significant at the 90% level were removed from the model equation by the backward elimination method (Ref 16). Ten terms were found to make significant contributions to the deposition efficiency

Table 2 ANOVA table for deposition efficiency (EfficiencyR)

Source	Sum of squares	df	Mean square	F value	*P*-value Prob > F	
Model	0.064	10	0.0064	28.8	<0.0001	Significant
A-HydrogenFR	0.0012	1	0.0012	5.6	0.0268	
C-SoluteFR	0.0023	1	0.0023	10.5	0.0035	
D-SolutionC	0.011	1	0.011	50.1	<0.0001	
E-DistanceNG	0.0098	1	0.0098	44.3	<0.0001	
F-StandOD	0.0042	1	0.0042	19.0	0.0002	
AF	0.0068	1	0.0068	30.8	<0.0001	
CD	0.0026	1	0.0026	11.7	0.0023	
CF	0.0043	1	0.0043	19.6	0.0002	
DF	0.0038	1	0.0038	17.22	0.0004	
F^2	0.017	1	0.017	79.0	<0.0001	
Residual	0.0051	23	0.00022			
Lack of fit	0.0047	18	0.00026	3.3	0.0917	Not significant
Pure error	0.00039	5	0.000078			
Cor total	0.069	33				

(EfficiencyR). The 10-term model for estimating deposition efficiency by coded and actual processing parameters (Ref 8, 9) can be expressed by Eq 1 and 2, respectively.

$$\begin{aligned}\text{EfficiencyR} = {} & 0.081 - \left(8.333 \times 10^{-3}\right) A + 0.011C \\ & + 0.025D + 0.023E - 0.015F - 0.021AF \\ & + 0.013D + 0.017CF + 0.015DF + 046F^2 \end{aligned} \quad \text{(Eq 1)}$$

$$\begin{aligned}\text{EfficiencyR} = {} & +2.84 + 0.14\text{HydrogenFR} - 0.095\text{SoluteFR} \\ & - 1.04\text{SolutionC} + 0.059 \quad \text{DistanceNG} - 0.72\text{StandOD} \\ & - 0.021\text{HydrogenFR.StandOD} + 0.068\text{SoluteFR.} \\ & \text{SolutionC} + 0.011\text{SoluteFR.StandOD} \\ & + 0.12\text{SolutionC.StandOD} + 0.046\text{StandOD}^2 \end{aligned} \quad \text{(Eq 2)}$$

From the model equations it can be seen that all processing parameters are included among the linear terms of the model, except for arc current (B-I); only the factor distance between nozzle and gun (E-DistanceNG) does not appear among the 2 factor interaction terms; and standoff distance (F-StandOD) is the only variable with a significant second-order effect. Thus the model equation indicates that standoff distance (F-StandOD) is the most important processing parameter. The analysis of variance (ANOVA) Table 2 shows the effects of the different terms in the model equation. Since the F values (signal to noise ratio) for standoff distance (F-StandOD) squared, solution precursor concentration (D-SolutionC), distance between nozzle and gun (E-DistanceNG), and interaction of gun arc voltage (A-HydrogenFR) and standoff distance (F-StandOD) are the largest in the ANOVA Table 2, these four have the most important effects on deposition efficiency (EfficiencyR) in the selected experimental area.

3.4.2 Quadratic Model for Porosity. By the same analysis as for deposition efficiency, the equations for predicting porosity (Porosity) in coded and actual variables were found to be expressed by Eq 3 and 4, respectively.

$$\begin{aligned}\text{Porosity} = {} & +35.88 - 6.77A - 3.03B - 1.58C + 1.27D \\ & + 0.72E + 1.89F - 0.69AB - 0.79AC \\ & + 2.39AD - 1.90AF - 4.61BF + 1.45CD \\ & + 1.00CE - 6.33DE - 2.20DF - 2.31EF \\ & + 2.61D^2 - 3.41E^2 + 3.76F^2 \end{aligned} \quad \text{(Eq 3)}$$

$$\begin{aligned}\text{Porosity} = {} & -621.31 + 17.22\text{HydrogenFR} + 1.11I \\ & - 5.22\text{SoluteFR} + 104.62\text{SolutionC} \\ & + 140.26\text{DistanceNG} + 67.73\ \text{StandOD} \\ & - 0.03\text{HydrogenFR.I} - 0.52\text{HydrogenFR.SoluteFR} \\ & + 19.13\text{HydrogenFR.SolutionC} \\ & - 1.89\text{HydrogenFR.StandOD} - 0.16\text{I.StandOD} \\ & + 7.72\ \text{SoluteFR.SolutionC} \\ & + 1.67\text{SoluteFR.DistanceNG} \\ & - 126.60\ \text{SolutionC.DistanceNG} \\ & - 17.58\ \text{SolutionC.StandOD} \\ & - 5.78\text{DistanceNG.StandOD} + 166.80\text{SolutionC}^2 \\ & - 21.31\ \text{DistanceNG}^2 + 3.76\text{StandOD}^2 \end{aligned} \quad \text{(Eq 4)}$$

There are 19 terms out of the 28 which have statistically significant effects on the porosity (Porosity), and remain in the quadratic equation. All six processing parameters appear among the linear terms, but the distance between nozzle and gun (E-DistanceNG) and solute flow rate (C-SoluteFR) are not statistically significant items as shown in the ANOVA Table 3; they were included in the linear part of the model since these two factors are involved in the interaction and/or second-order terms of the model. Solution concentration (D-SolutionC), standoff distance (F-StandOD), distance between nozzle and gun (E-DistanceNG) and hydrogen flow rate (A-HydrogenFR) appear 6, 6, 5, and 5 times, respectively, in the equations; therefore, they are important processing parameters for controlling the porosity of fabricated coatings. The ANOVA Table 3 shows that the F values related to

Table 3 ANOVA table for porosity (Porosity)

Source	Sum of squares	df	Mean square	F value	*P*-value Prob > F	
Model	959.69	19	50.51	41.3	<0.001	Significant
A-HydrogenFR	91.57	1	91.57	74.9	<0.001	
B-I	165.01	1	165.01	135.1	<0.001	
C-SoluteFR	5.01	1	5.01	4.1	0.062	
D-SolutionC	28.88	1	28.88	23.6	<0.001	
E-DistanceNG	1.02	1	1.027	0.8	0.374	
F-StandOD	64.22	1	64.22	52.5	<0.001	
AB	7.58	1	7.58	6.2	0.025	
AC	10.10	1	10.10	8.2	0.012	
AD	10.16	1	10.16	8.3	0.012	
AF	57.69	1	57.69	47.2	<0.001	
BF	37.70	1	37.70	30.8	<0.001	
CD	33.54	1	33.54	27.4	<0.001	
CE	16.06	1	16.06	13.1	0.002	
DE	71.23	1	71.23	58.3	<0.001	
DF	77.29	1	77.29	63.3	<0.001	
EF	85.71	1	85.71	70.1	<0.001	
D^2	19.46	1	19.46	15.9	0.001	
E^2	33.33	1	33.33	27.3	<0.001	
F^2	40.62	1	40.62	33.2	<0.001	
Residual	17.09	14	1.22			
Lack of fit	9.53	9	1.05	0.70	0.697	Not significant
Pure error	7.56	5	1.51			
Cor total	976.79	33				

arc current (B-I), hydrogen flow rate (A-HydrogenFR), interaction of distance between nozzle and gun (E-DistanceNG) and standoff distance (F-StandOD), interaction of solution concentration (D-SolutionC) and standoff distance (F-StandOD), interaction of solution concentration (D-SolutionC) and distance between nozzle and gun (E-DistanceNG), and standoff distance (F-StandOD) are larger than those related to the other items. So these six items are critical for determining the porosity of the fabricated coatings.

3.4.3 Model Adequacy Checking. Model adequacy checks were made by residual analysis, predicted versus actual plots, testing for lack of fit, and R squared calculations. A residual e_i is the difference between the measured experimental response y_i and the reponse $\hat{y}_i$ predicted by the model equation, $e_i = y_i - \hat{y}_i (i = 1, 2 \ldots n)$. According to the basic assumptions of experimental design, the residuals should be normally distributed (Ref 8, 9), otherwise model inadequacy is indicated. A check of the normality assumption is usually done by constructing a normal probability plot of the residuals. If the residuals fall approximately on a straight line, the normal distribution of residuals is confirmed. Analysis indicates that the residuals are on the lines and concentrated on the center parts of the lines, showing that there are no problems with the residual normalities. Figure 2 is the normal plot of residuals for the model of deposition efficiency.

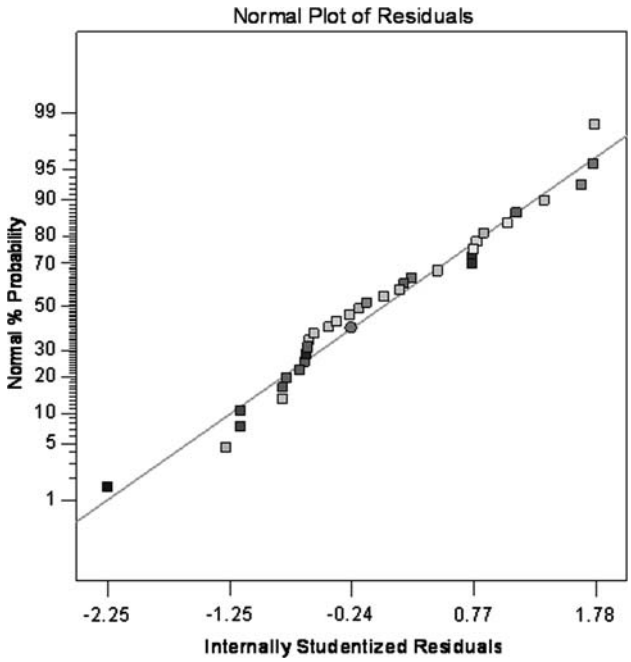

Fig. 2 Normal plot of residuals for model of deposition efficiency

The predicted versus actual plot is a graph of the measured versus the predicted response values. The data points should be split evenly by the 45-degree line or ideally all points should fall on the line. Figure 3 is the predicted versus actual plot for porosity (Porosity). The plot for deposition efficiency (EfficiencyR) has a similar distribution, demonstrating that the models appear to provide an excellent description of the effects of the various process parameters.

Testing for lack of fit is to examine if the model fits the data by calculating the lack of fit F value. The larger the F value, the more likely that the model does not adequately fit the data. The lack of fit F values for models of deposition efficiency (EfficiencyR) and porosity (Porosity) are

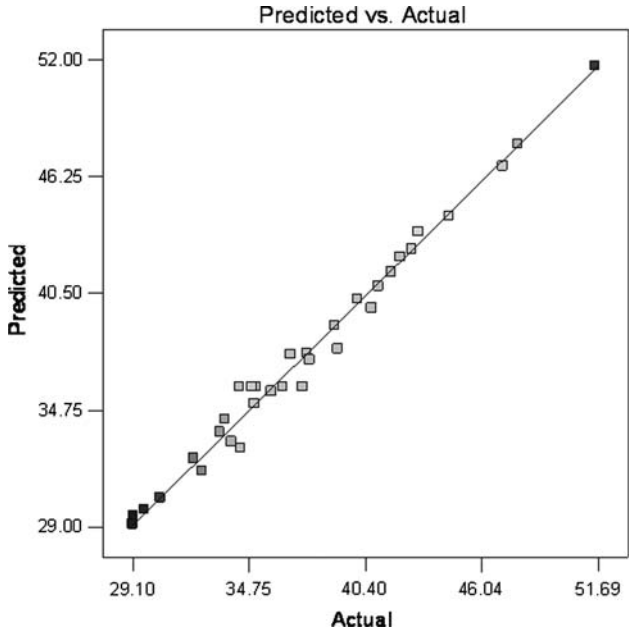

Fig. 3 Predicted versus actual plots for model of Porosity (Porosity)

	EfficiencyR	Porosity, %
Predicted	0.235	40
Measured	0.220	43

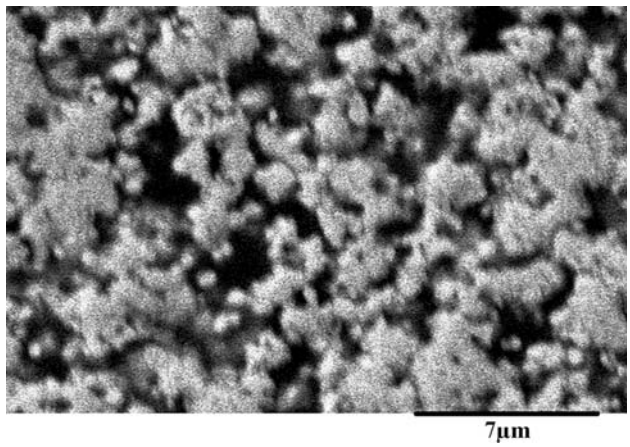

Fig. 4 SEM micrograph of a cross section of the coating deposited with optimized conditions

3.3 and 0.7 as shown in Table 2 and 3, respectively, which indicate that the models are acceptable.

R-Squared is the part of the variation about the mean that is explained by the fitted model. The calculations of R-Squared are described in Ref 8, 9. The R-Squared values for deposition efficiency (EfficiencyR) and porosity (Porosity) are 0.93 and 0.98, respectively. To overcome the increase in R-Squared with the addition of insignificant terms to the model, Adjusted R-Squared values are used. The Adjusted R-Squared values for deposition efficiency (EfficiencyR) and porosity (Porosity) are 0.89 and 0.96, respectively, meaning the two models are satisfactory.

3.5 Process Optimization

Within the experimental area in which NiO-YSZ deposits can be produced, the deposition process was optimized by the experiment design software (Design Expert 7.0.2) based on the analyses described in previous sections. This optimization process can also be done manually by using a desirability function (Ref 9). According to the microstructure requirements for a SOFC anode, the porosity (Porosity) target was 40%. The deposition efficiency (EfficiencyR) was desired to be maximum. The optimization analysis on the above conditions generated 59 processing parameter combinations and predicted responses as described in Ref 15. Considering the operational limits of the equipment, the parameter combination used to deposit a coating was: hydrogen flow rate = 1l/min; arc current = 610 A; solute flow rate = 6.9 g/min; solution concentration = 0.5 M; distance between nozzle and gun = 1.69 cm; standoff distance = 8 cm. Characterization of this coating yielded the following results:

Figure 4 is an SEM micrograph of a polished cross section of the coating deposited with the selected conditions, illustrating that the coating is very porous. The results above indicate that the optimized process parameters can be used to generate coatings with the desired porosity and at relatively high-deposition efficiency.

4. Understanding the Results of Statistical Design of Experiments

Relations between the processing parameters and the responses, i.e., the deposition efficiency (EfficiencyR) and the porosity (Porosity) as described by Eq 1 and 3, respectively, were obtained in the optimization of Ni-YSZ coatings. Although each response is a function of the processing parameters, it is very difficult to explain why each term takes the exact form it has in the functions. This difficulty arises from several considerations including the fact that the physical mechanism determining the relation between the response and each term in the function was not investigated directly and that some effects from higher order interactions may be confounded with the terms included in the models since only a fractional factorial design of experiment was used in the optimizations reported here. Therefore, in this section possible physical explanations for the effects described by only the linear terms in each model will be discussed based on the experimental observations and theoretical considerations. Other terms in the functions will be interpreted where possible. Since the equations with coded factors are independent of the numerical values of factors, they will be used as the basis of the discussion in the following subsections.

4.1 Deposition Efficiency

The deposition efficiency (EfficiencyR) is expressed by Eq 1 according to the analysis in the optimization of Ni-YSZ coating deposition. There are five terms, hydrogen flow rate (A), solution flow rate (C), solution concentration (D), distance between nozzle and gun (E) and standoff distance (F), in the linear part of the equation. The deposition efficiency (EfficiencyR) increases with the increase of solution flow rate (C), solution concentration (D), and distance between nozzle and gun (E). It decreases with the increase of hydrogen flow rate (A) and standoff distance (F).

A larger hydrogen flow rate (A) will increase the plasma gun voltage and generates a higher temperature and higher velocity plasma jet (Ref 17, 18). The higher temperature may vaporize more solute, decreasing the deposition efficiency (EfficiencyR), while the higher velocity would produce smaller droplets and smaller agglomerates as discussed in Ref 15. Small synthesized particles will follow the gas flow streams and may not impact onto the substrates, reducing the deposition efficiency (EfficiencyR) again. So the deposition efficiency (EfficiencyR) decreases with the increase of hydrogen flow rate (A).

As the solution flow rate (C) and solution concentration (D) increase, the mass density of synthesized material in the plasma jet would rise, which will result in the increase of probability of particle collisions. As a result, the agglomerates formed in the plasma jet would be larger (Ref 15), increasing the stopping distance and the deposition efficiency (EfficiencyR) as described in Ref 15. Therefore, the deposition efficiency (EfficiencyR) increases with the increase of solution flow rate (C) and solution concentration (D).

Increasing distance between nozzle and gun (E) is equal to decreasing plasma temperature and gas velocity. The lower temperature will vaporize less solute while the lower gas velocity will produce larger droplets and larger agglomerates as discussed in Ref 15. Therefore, increasing the distance between nozzle and gun (E) would increase deposition efficiency (EfficiencyR).

A longer standoff distance (F) allows a longer residence time of the synthesized materials and more probability of synthesized particle collisions, promoting the formation of larger agglomerates (Ref 15); therefore, a longer standoff distance (F) could increase deposition efficiency (EfficiencyR). However, a longer standoff distance (F) will also reduce the velocity of the synthesized particles, reducing the stopping distance and the deposition efficiency (EfficiencyR). The F term in Eq 1 (minus sign) indicates that the deposition efficiency (EfficiencyR) decreases with the increase of standoff distance (F), suggesting the velocity of synthesized particles is too low for impact onto the substrates (Ref 15).

4.2 Porosity

There are six terms in the linear part of Eq 3, which estimates the porosity (Porosity) of the fabricated Ni-YSZ coatings. However, the solution flow rate (C) and distance between nozzle and gun (E) are not significant. The porosity (Porosity) increases with the increase of solution concentration (D) and standoff distance (F) while it decreases when hydrogen flow rate (A) and gun current (B) increase.

According to the observations in Ref 15, there are two kinds of pores in the fabricated Ni-YSZ coatings, i.e., large pores between agglomerates and fine pores inside the agglomerates. The large pores, which account for a large fraction of the total porosity (Ref 15), are formed by stacking of the partially molten agglomerates.

A larger hydrogen flow rate (A) and gun current (B) will generate a higher temperature and velocity plasma jet (Ref 17, 18). The higher velocity would produce smaller droplets (Ref 19) and smaller agglomerates, which result in the formation of smaller pores between agglomerates. The higher temperature of the plasma jet would make the smaller agglomerates more molten and more deformable during impact onto the substrates, decreasing the porosity (Porosity). Therefore, the porosity (Porosity) decreases with increase of hydrogen flow rate and plasma gun current.

A higher solution concentration (D) increases the mass density of the particles in the plasma jet, resulting in more collisions of particles and larger and less molten agglomerates (Ref 15), promoting the formation of large pores between agglomerates. In addition, a lower concentration precursor tends to produce denser agglomerates (Ref 20). Therefore the porosity (Porosity) increases with the increase of solution concentration (D).

A longer standoff distance (F) increases the probability of synthesized particle collisions, forming larger agglomerates (Ref 15). Since the temperature of the plasma at impact is lower at longer standoff distance and the larger agglomerates have a higher heat capacity, the larger agglomerates would be relatively less molten, promoting the formation of coatings with higher porosity; therefore, the porosity (Porosity) increases with the increase of standoff distance (F).

A plasma gun operating at low power will generate lower temperature and velocity plasma gases, which promotes generation of larger agglomerates (Ref 15). Larger agglomerates would be less molten and less deformable during impact, therefore the low power coating would have larger porosity. This conclusion is consistent with the fact that there is a minus sign before the term describing the effect of the interaction between hydrogen flow rate (A), which determines gun voltage, and gun current (B) in Eq 3.

5. Conclusion

Quadratic models for predicting deposition efficiency and porosity were obtained by the small central composite experimental design technique. The model adequacy checking indicated that the models are statistically satisfactory. The models were used successfully to select

process parameters which generated coatings with the desired porosity at a relatively high-deposition efficiency.

Physical-based explanations of the empirical relations between the processing parameters and the responses, i.e., the deposition efficiency (EfficiencyR) and the porosity (Porosity), were discussed with reference to experimental observations and theoretical considerations.

Acknowledgments

This project was financially supported by Natural Science and Engineering Research Council (NSERC) of Canada. The authors would like to express their gratitude to Dr. L. Pershin and Mr. T. Li in our laboratory for their kind help in the plasma spray experiments.

References

1. H. Wang, J. Williams, K.D. Vuong, C.Q. Shen, V. Wu, D.H. Lee, R.A. Condrate, and X.W. Wang, RF Plasma Fabrication of Nano-Scaled Ceramic Oxides for Energy Devices. *Proceedings of the 30th Intersociety Energy Conversion Engineering Conference. Orlando, July 30-August 4, 1995,* p 295-300
2. M. Gell, L. Xie, X. Ma, E.H. Jordan, and N.P. Padture, Highly Durable Thermal Barrier Coatings Made by the Solution Precursor Plasma Spray Process, *Surf. Coat. Technol.*, 2004, **177-178**, p 97-102
3. Y. Shan, T.W. Coyle, and J. Mostaghimi, Numerical Simulation of Droplet Breakup and Collision in the Solution Precursor Plasma Spraying, *J. Therm. Spray Technol.*, 2007, **16**(5-6), p 698-704
4. F. Gitzhofer, M.-E. Bonneau, and M. Boulos, Double Doped Ceria Electrolyte Synthesized by Solution Plasma Spraying with Induction Plasma Technology, *Thermal Spray 2001: New Surfaces for a New Millennium*. C.C. Berndt, D.A. Dhor, and E.F. Lugscheider, Eds., (Materials Park, Ohio, USA), ASM International, 2001, p 61-68
5. S.H. Miralai, D. Morvan, J. Amouroux, A. Naoumidis, H. Nickel, and R. Avni, Perovskite Thin Coating Deposition from Aqueous Nitrate Solutions of La and Mn in a Low Pressure Plasma Expanded Through a Nozzle, *12th International Symposium on Plasma Chemistry (ISPC 12)*. Vol. 2, Minneapolis, August 21-25, 1995, p 1999-2004
6. Y. Wang and T.W. Coyle, Solution Precursor Plasma Spray of Nickel-Yittia Stabilized Zirconia Anodes for Solid Oxide Fuel Cell Application, *J. Therm. Spray Technol.*, 2007, **16**(5-6), p 898-904
7. K. Chien and T.W. Coyle, Rapid and Continuous Deposition of Porous Nanocrystalline SnO_2 Coating with Interpenetrating Pores for Gas Sensor Applications, *J. Therm. Spray Technol.*, 2007, **16**(5-6), p 886-892
8. G.E.P. Box and N.R. Draper, *Empirical Model-Building and Response Surfaces*, John Wiley & Sons, Inc., New York, 1986
9. R.H. Myers and D.C. Montgomery, *Response Surface Methodology*, 2nd ed., John Wiley & Sons, Inc., New York, 2002
10. R. Kingswell, K.T. Scott, and L.L. Wassell, Optimizing the Vacuum Plasma Spray Deposition of Metal, Ceramic and Cermet Coatings Using Designed Experiments, *J. Therm. Spray Technol.*, 1993, **2**(2), p 179-186
11. C.J. Li, G.C. Ji, and Y. Wang, Effect of Powder Type on the Relationship Between Spray Parameters and Properties of HVOF Sprayed Cr_3C_2-NiCr Coatings, Thermal Spray: Meeting the Challenges of the 21st Century, *Proceedings of the 15th International Thermal Spray Conference*, C. Coddet, Ed., (Nice, France), ASM International, 1998, p 287-292
12. F. Azarmi, T.W. Coyle, and J. Mostaghimi, Optimization of Atmospheric Plasma Spray Process Parameters Using a Design of Experiment for Alloy 625 Coatings, *J. Therm. Spray Technol.*, 2008, **18**, p 1-12
13. C. Pierlot, L. Pawlowski, M. Bigan, and P. Chagnon, Design of Experiments in Thermal Spraying: A Review, *Surf. Coat. Technol.*, 2008, **202**, p 4483-4490
14. H.O. Hartley, Smallest Composite Designs for Quadratic Response Surfaces, *Biometrics*, 1959, **15**(4), p 611-624
15. Y. Wang, ''Deposition of Solid Oxide Fuel Cell Electrodes by Solution Precursor Plasma spray,'' Ph. D. Thesis, University of Toronto, 2008
16. http://www.statease.com/software.html. Accessed 2006
17. M.P. Planche, J.F. Coudert, and P. Fauchais, Velocity Measurements for Arc Jets Produced by a DC Plasma Spray Torch, *Plasma Chem. Plasma Process.*, 1998, **18**(2), p 263-283
18. S. Semenov and B. Cetegen, Spectroscopic Temperature Measurement in Direct Current Arc Plasma Jets Used in Thermal Spray Processing of Materials, *J. Thermal Spray Technol.*, 2001, **10**, p 326-336
19. M. Pilch and C.A. Erdman, Use of Breakup Time Data and Velocity History Data to Predict the Maximum Size of Stable Fragments for Acceleration-Induced Breakup of a Liquid Droplet, *Int. J. Multiphase Flow*, 1987, **13**(6), p 741-757
20. A. Curav, T. Kodas, T. Pluym, and Y. Xiong, Aerosol Processing of Materials, *Aerosol Sci. Technol.*, 1993, **19**, p 411-452